Available online at www.sciencedirect.com
ScienceDirect
Journal of Computational and Applied Mathematics 203 (2007) 219–236
JOURNAL OF COMPUTATIONAL AND APPLIED MATHEMATICS
www.elsevier.com/locate/cam

High resolution of 2D natural convection in a cavity by the DQ method

D.C. Lo[a,*], D.L. Young[b], C.C. Tsai[c]

[a] *Department of Animation Design and Game Programming, Toko University, Chia-Yi County, 61363, Taiwan*
[b] *Department of Civil Engineering and Hydrotech Research Institute, National Taiwan University, Taipei 10617, Taiwan*
[c] *Department of Information Technology, Toko University, Chia-Yi County, 61363, Taiwan*

Received 16 November 2005; received in revised form 15 February 2006

Abstract

In this paper, the differential quadrature method (DQ) is applied to solve the benchmark problem of 2D natural convection in a cavity by utilizing the velocity–vorticity form of the Navier–Stokes equations, which is governed by the velocity Poisson equation, continuity equation and vorticity transport equation as well as energy equation. The coupled equations are simultaneously solved by imposing the vorticity definition at boundary without any iterative procedure. The present model is properly utilized to obtain results in the range of Rayleigh number (10^3–10^7) and H/L aspect ratios varying from 1 to 3. Nusselt numbers computed for $10^3 \leqslant Ra \leqslant 10^7$ in a cavity show excellent agreement with the results available in the literature. Additionally, the detailed features of flow phenomena such as velocity, temperature, vorticity, and streamline plots are also delineated in this work. Thus, it is convinced that the DQ method is capable of solving coupled differential equations efficiently and accurately.

Keywords: Natural convection; Differential quadrature; Velocity–vorticity form; Aspect ratios; Nusselt numbers

1. Introduction

Computational fluid dynamics (CFD) finds wide range of applications in sciences and engineering. Computation of incompressible Navier–Stokes equations is the most significant area in CFD. The velocity–vorticity form of the Navier–Stokes equations has been developed in [5] as an alternative scheme without involving the pressure term. The main advantage of the velocity–vorticity formulation is that its numerical formulation is independent of whether or not the reference frame is inertial. To be precise, the vorticity is one of the field variables, thus velocity–vorticity formulation can be exploited to study vortex dominated flows no matter 2D or 3D flow is considered. Furthermore, the extension of 3D flow is also straightforward while the velocity–vorticity formulation is used. When the incompressible Navier–Stokes equations are solved in the velocity–vorticity form, the numerical algorithm varies depending upon how the vorticity term is treated with respect to the vorticity transport equation especially for the vorticity values at the boundary wall. In many practical problems vorticity values at the boundary wall are one of the variables to be considered for design purpose. Thereby, the velocity–vorticity form of the Navier–Stokes equations is an alternative

* Corresponding author. Tel.: +886 937901143.
E-mail address: loderg@ntu.edu.tw (D.C. Lo).

0377-0427/$ - see front matter © 2006 Elsevier B.V. All rights reserved.
doi:10.1016/j.cam.2006.03.021

Nomenclature

$A_{i,k}^{(l)}$	weighting coefficients for the lth order derivatives of the function with respect to x
$B_{j,k}^{(m)}$	weighting coefficients for the mth order derivatives of the function with respect to y
L	number of grid points in the x direction
M	number of grid points in the y direction
Nu_{avg}	the average Nusselt number on the boundary of the cavity at $x = 0$
$Nu_{\max}$	the maximum value of local Nusselt number on the boundary of the cavity at $x = 0$
$Nu_{\min}$	the minimum value of local Nusselt number on the boundary of the cavity at $x = 0$
Pr	Prandtl number
Ra	Rayleigh number
t	dimensionless time
T	dimensionless temperature
u, v	dimensionless velocities in the x and y directions
x, y	dimensionless Cartesian coordinates
ω	dimensionless vorticity in the z direction
H/L	aspect ratios of height and length
Γ	problem boundary
Ω	computational domain

scheme in many CFD applications. However, the number of field variables increases from three to six for the cases of 3D Navier–Stokes equations, which may be a disadvantage. In order to circumvent the pitfalls associated with the vorticity values at the boundary, a global DQ method is employed to compute vorticity boundary values implicitly without using any iterative procedure. As pointed out in [3] the satisfaction of the continuity equation reduces to enforcing the vorticity definition at the boundary in terms of curl of the velocity field. The Navier–Stokes equations in velocity–vorticity form indicate that vorticity is created at the boundary by satisfying the velocity boundary conditions [1]. The definition of vorticity is given by the curl of the velocity field. Consequently, in order to correctly satisfy the vorticity definition at the boundary, computation of accurate velocity gradients or the vorticity values at the boundary are very crucial. As indicated by the investigators [7,17,9], in order to enforce the solenoidality of vorticity in the computation of flow problems, the vorticity transport equations have to be solved with the vorticity values at the boundary.

It is well known that the curl of vorticity definition results in the kinematic velocity Poisson equations for an incompressible fluid flow. Additionally, the curl of the momentum equations in primitive variable form gives rise to the dynamic vorticity transport equations. A detailed discussion was briefly presented in [7]. It should be noted that the solenoidality of velocity field can be assured only by coupling the kinematic and dynamic equations. In the present work, the velocity u in the x direction is solved by the velocity Poisson equation and the velocity v in the y direction is obtained from the differentiated form of the continuity equation, hence assuring a divergence-free velocity field. For the variables of the vorticity and temperature field, the vorticity transport equation and energy equation are used for solving the vorticity and temperature variables of the flow field. When higher-order approximation is discretized to compute all flow variables, also a numerical coupling between the velocity, vorticity and temperature is required to satisfy the solenoidality constraint of the velocity field. Therefore the motivation for the present work originated from the fact that how to enforce the vorticity definition accurately as the curl of velocity both at the interior and at the boundaries of the computational domain. By coupling the entire field variables the vorticity boundary values can be computed implicitly from the velocity fields and enforced at the boundary nodes.

In recent years, the DQ method is becoming a powerful numerical scheme to solve partial differential equations with higher-order accuracy. The DQ method was first developed in [2] to approximate the derivative of a smooth function using a higher-order polynomial. The application of the DQ method has been successfully implemented for solving engineering problems by many researchers [13,14,11]. Shu and Xue [14] applied generalized DQ method to solve the natural convection in a square cavity. Two boundary conditions (Dirichlet and Neumann type) were discussed therein for the streamfunction at each boundary. Recently, a number of meshless methods have been developed to solve natural convection problems. Shu et al. [12] developed a local radial basis function-based differential quadrature method and its

application to the simulation of natural convection in a square cavity. Additionally, the local radial interpolation method was developed in [19] for solving 2D natural convection problems with enclosed domain of different geometries. Ding et al. [4] also presented a meshless method based on the use of a weighted least-square approximation to solve 2D natural convection in a square cavity. Natural convection in a differentially heated enclosure is very popular problem as a test case to demonstrate the capability of any proposed numerical algorithm. The reason for selecting this problem is to prove the efficiency and accuracy of the proposed coupled numerical scheme to solve governing equations for vortex dominated flow. Since the vorticity transport equation is coupled to the energy equation through the buoyancy force, we choose this problem to test the proposed coupled numerical algorithm. The four field variables, two velocities, one vorticity, and one temperature are solved at the same time using a coupled numerical technique.

The proposed numerical scheme is applied to determine the velocity, vorticity and temperature variations for a natural convection problem in a differentially heated enclosure for Rayleigh number range of 10^3–10^7 and H/L aspect ratios varying from 1 to 3. Comparisons of the present results with those obtained by other numerical schemes are presented.

2. Differential quadrature method

The DQ method replaces a given spatial partial derivative of a function $f(x)$ by a linear weighted sum of the function values at the discrete sample points considered along the coordinate direction. As a result, the given partial differential equation reduces to a set of algebraic equations. Thereby the numerical solution of partial differential equations can be solved by the DQ method. This method has been briefly presented in Refs. [2,13,11]. For a function of two variables $f(x, y)$ the lth order derivatives and mth order derivatives of the function with respect to x and y can be obtained as [13,11]

$$f_x^{(l)}(x_i, y_j) = \sum_{k=1}^{L} A_{i,k}^{(l)} f(x_k, y_j), \quad l = 1, 2, \ldots, L-1, \tag{1a}$$

$$f_y^{(m)}(x_i, y_j) = \sum_{k=1}^{M} B_{j,k}^{(m)} f(x_i, y_k), \quad m = 1, 2, \ldots, M-1$$
$$\text{for } i = 1, 2, \ldots, L, \quad j = 1, 2, \ldots, M, \tag{1b}$$

where L, M are the numbers of grid points in the x, y direction, respectively, $A_{i,k}^{(l)}$, $B_{j,k}^{(m)}$ are the weighting coefficients. For the first-order derivatives, the weighting coefficients $A_{i,k}^{(1)}$, $B_{j,k}^{(1)}$ can be obtained as follows:

$$A_{i,j}^{(1)} = \frac{L^{(1)}(x_i)}{(x_i - x_j)L^{(1)}(x_j)}, \quad i, j = 1, 2, \ldots, L, \text{ but } j \neq i, \tag{2a}$$

$$B_{i,j}^{(1)} = \frac{M^{(1)}(y_i)}{(y_i - y_j)M^{(1)}(y_j)}, \quad i, j = 1, 2, \ldots, M, \text{ but } j \neq i, \tag{2b}$$

where

$$L^{(1)}(x_i) = \prod_{j=1, j\neq i}^{L} (x_i - x_j), \quad M^{(1)}(y_i) = \prod_{j=1, j\neq i}^{M} (y_i - y_j). \tag{3}$$

Similarly the weighting coefficients for the lth order derivatives and mth order derivatives of the function with respect to x and y can be obtained as

$$A_{i,j}^{(l)} = l\left(A_{i,i}^{(l-1)} A_{i,j}^{(1)} - \frac{A_{i,j}^{(l-1)}}{x_i - x_j}\right) \quad \text{for } i, j = 1, 2, \ldots, L, \text{ but } j \neq i, \quad l = 2, 3, \ldots, L-1, \tag{4a}$$

$$B_{i,j}^{(m)} = m\left(B_{i,i}^{(m-1)} B_{i,j}^{(1)} - \frac{B_{i,j}^{(m-1)}}{y_i - y_j}\right) \quad \text{for } i, j = 1, 2, \ldots, M, \text{ but } j \neq i, \quad m = 2, 3, \ldots, M-1. \tag{4b}$$

When $j = i$, the weighting coefficients are written as

$$A_{i,i}^{(l)} = -\sum_{j=1, j\neq i}^{L} A_{i,j}^{(l)}, \quad i = 1, 2, \ldots, L, \;\; l = 1, 2, \ldots, L-1, \tag{5a}$$

$$B_{i,i}^{(m)} = -\sum_{j=1, j\neq i}^{M} B_{i,j}^{(m)}, \quad i = 1, 2, \ldots, M, \;\; m = 1, 2, \ldots, M-1. \tag{5b}$$

It is quite important to note that the weighting coefficients of the second- and higher-order derivatives can be computed from the first-order derivatives themselves.

3. Governing equations and boundary conditions

In the case of natural convection problems, the Navier–Stokes equations include the buoyancy force generated as a result of fluid density difference caused by the temperature difference. The buoyancy term is computed based on the Boussinesq approximation. By taking the curl of the primitive variable form of the Navier–Stokes equations for natural convection and making use of the vorticity definition, the velocity–vorticity form of the natural convection equations can be derived as follows:

Velocity equations

$$\nabla^2 u = -\frac{\partial \omega}{\partial y}, \tag{6}$$

$$\frac{\partial^2 u}{\partial x\, \partial y} + \frac{\partial^2 v}{\partial y^2} = 0. \tag{7}$$

We use the continuity equation (Eq. (7)) instead of the velocity Poisson equation ($\nabla^2 v = \partial\omega/\partial x$) to solve velocity component v in order to reduce the CPU time for the flow computation as recommendation in [18].

Vorticity transport equation

$$\frac{\partial \omega}{\partial t} + u\frac{\partial \omega}{\partial x} + v\frac{\partial \omega}{\partial y} = Pr\nabla^2\omega + Ra\, Pr\frac{\partial T}{\partial x}. \tag{8}$$

Energy equation

$$\frac{\partial T}{\partial t} + u\frac{\partial T}{\partial x} + v\frac{\partial T}{\partial y} = \nabla^2 T, \tag{9}$$

where L, α/L, α/L^2, L^2/α and $T = (\theta - \theta_c)/(\theta_h - \theta_c)$ are used as scale factors for length, velocity, vorticity, time, and temperature in the above non-dimensional form of the governing equations. The non-dimensional parameters are defined as $Ra = g\beta\Delta T L^3/\alpha\upsilon$ and $Pr = \upsilon/\alpha$. The velocity Poisson and continuity equations (6), (7) remain unaffected as they represent the kinematic condition of the flow field. Eqs. (8), (9) with ω as vorticity and T as the scalar temperature field as well as velocity field (Eqs. (6), (7)) are the final form of the governing equations to be solved in the domain Ω with the specified boundary conditions for velocity, vorticity and temperature on the solid boundary Γ.

In Eqs. (6), (7), u and v are the velocities in x and y directions, respectively, in a computational domain Ω surrounded by a boundary Γ. We seek a solution in the domain Ω, which enforces the Dirichlet boundary conditions of velocity given by

$$\vec{u} = (u, v) = \vec{u}_b \tag{10}$$

and the corresponding vorticity values on the boundary can be obtained using the definition given as

$$\omega = \frac{\partial v}{\partial x} - \frac{\partial u}{\partial y}. \tag{11}$$

The Dirichlet and Neumann boundary conditions of present cases for temperature are as follows:

$$T = T_b, \tag{12a}$$

$$\frac{\partial T}{\partial y} = 0. \tag{12b}$$

4. Formulations by DQ method

The velocity equations (6), (7) can be approximated by the DQ method as follows:

$$\sum_{k=1}^{L} A_{i,k}^{(2)} u_{k,j} + \sum_{k=1}^{M} B_{j,k}^{(2)} u_{i,k} + \sum_{k=1}^{M} B_{j,k}^{(1)} \omega_{i,k} = 0, \tag{13}$$

$$\sum_{k1=1}^{L} A_{i,k1}^{(1)} \sum_{k2=1}^{M} B_{j,k2}^{(1)} u_{k1,k2} + \sum_{k=1}^{M} B_{j,k}^{(2)} v_{i,k} = 0. \tag{14}$$

For the vorticity transport equation, the non-linear term is treated explicitly, the viscous term is treated implicitly, as well as the time derivative is discretized by a second-order time stepping of finite difference type (see Refs. [16,6]) by the global method of DQ approximation. The vorticity transport equation can be discretized as the following formula:

$$\frac{3\omega^{n+1} - 4\omega^n + \omega^{n-1}}{2\Delta t} + 2\left(u\frac{\partial \omega}{\partial x} + v\frac{\partial \omega}{\partial y}\right)^n - \left(u\frac{\partial \omega}{\partial x} + v\frac{\partial \omega}{\partial y}\right)^{n-1} - Pr\nabla^2\omega^{n+1} - Ra\,Pr\left(\frac{\partial T}{\partial x}\right)^{n+1} = 0. \tag{15}$$

By using the DQ approximation the above equation can be expressed as

$$\begin{aligned}
&\left(\frac{3}{2\Delta t}\right)\omega_{i,j}^{n+1} - Pr\left(\sum_{k=1}^{L} A_{i,k}^{(2)}\omega_{k,j} + \sum_{k=1}^{M} B_{j,k}^{(2)}\omega_{i,k}\right)^{n+1} - Ra\,Pr\sum_{k=1}^{L} A_{i,k}^{(1)}(T_{k,j})^{n+1} \\
&\quad = \left(\frac{4}{2\Delta t}\right)\omega_{i,j}^{n} - \left(\frac{1}{2\Delta t}\right)\omega_{i,j}^{n-1} - 2\left(u_{i,j}\sum_{k=1}^{L} A_{i,k}^{(1)}\omega_{k,j} + v_{i,j}\sum_{k=1}^{M} B_{j,k}^{(1)}\omega_{i,k}\right)^{n} \\
&\qquad + \left(u_{i,j}\sum_{k=1}^{L} A_{i,k}^{(1)}\omega_{k,j} + v_{i,j}\sum_{k=1}^{M} B_{j,k}^{(1)}\omega_{i,k}\right)^{n-1}.
\end{aligned} \tag{16}$$

Similarly, the energy equation is written as

$$\begin{aligned}
\left(\frac{3}{2\Delta t}\right)T_{i,j}^{n+1} - \left(\sum_{k=1}^{L} A_{i,k}^{(2)}T_{k,j} + \sum_{k=1}^{M} B_{j,k}^{(2)}T_{i,k}\right)^{n+1} &= \left(\frac{4}{2\Delta t}\right)T_{i,j}^{n} - \left(\frac{1}{2\Delta t}\right)T_{i,j}^{n-1} \\
&\quad - 2\left(u_{i,j}\sum_{k=1}^{L} A_{i,k}^{(1)}T_{k,j} + v_{i,j}\sum_{k=1}^{M} B_{j,k}^{(1)}T_{i,k}\right)^{n} \\
&\quad + \left(u_{i,j}\sum_{k=1}^{L} A_{i,k}^{(1)}T_{k,j} + v_{i,j}\sum_{k=1}^{M} B_{j,k}^{(1)}T_{i,k}\right)^{n-1}.
\end{aligned} \tag{17}$$

The algebraic equations (13)–(14), (16)–(17) represent the DQ form of the governing equations for the velocity, vorticity and temperature. By combining the coefficient matrices of all the field variables, the following global matrix form is

obtained for the coupled solution algorithm:

$$\begin{bmatrix} A_1 & 0 & A_2 & 0 \\ B_1 & B_2 & 0 & 0 \\ 0 & 0 & C_1 & C_2 \\ 0 & 0 & 0 & D_1 \end{bmatrix} \begin{Bmatrix} u \\ v \\ \omega \\ T \end{Bmatrix} = \begin{Bmatrix} f_u \\ f_v \\ f_\omega \\ f_T \end{Bmatrix}. \tag{18}$$

The submatrices and the load vectors can be written as

$$[A_1] = \sum_{k=1}^{L} A_{i,k}^{(2)} + \sum_{k=1}^{M} B_{j,k}^{(2)}, \quad [A_2] = \sum_{k=1}^{M} B_{j,k}^{(1)},$$

$$[B_1] = \sum_{k1=1}^{L} A_{i,k1}^{(1)} \sum_{k2=1}^{M} B_{j,k2}^{(1)}, \quad [B_2] = \sum_{k=1}^{M} B_{j,k}^{(2)},$$

$$[C_1] = \left(\frac{3}{2\Delta t}\right) - Pr\left(\sum_{k=1}^{L} A_{i,k}^{(2)} + \sum_{k=1}^{M} B_{j,k}^{(2)}\right), \quad [C_2] = -Ra\,Pr \sum_{k=1}^{L} A_{i,k}^{(1)},$$

$$[D_1] = \left(\frac{3}{2\Delta t}\right) - \left(\sum_{k=1}^{L} A_{i,k}^{(2)} + \sum_{k=1}^{M} B_{j,k}^{(2)}\right),$$

$$[f_u] = 0, \quad [f_v] = 0,$$

$$[f_\omega] = \left(\frac{4}{2\Delta t}\right)\omega_{i,j}^{n} - \left(\frac{1}{2\Delta t}\right)\omega_{i,j}^{n-1} - 2\left(u_{i,j}\sum_{k=1}^{L} A_{i,k}^{(1)}\omega_{k,j} + v_{i,j}\sum_{k=1}^{M} B_{j,k}^{(1)}\omega_{i,k}\right)^{n} + \left(u_{i,j}\sum_{k=1}^{L} A_{i,k}^{(1)}\omega_{k,j} + v_{i,j}\sum_{k=1}^{M} B_{j,k}^{(1)}\omega_{i,k}\right)^{n-1},$$

$$[f_T] = \left(\frac{4}{2\Delta t}\right)T_{i,j}^{n} - \left(\frac{1}{2\Delta t}\right)T_{i,j}^{n-1} - 2\left(u_{i,j}\sum_{k=1}^{L} A_{i,k}^{(1)}T_{k,j} + v_{i,j}\sum_{k=1}^{M} B_{j,k}^{(1)}T_{i,k}\right)^{n} + \left(u_{i,j}\sum_{k=1}^{L} A_{i,k}^{(1)}T_{k,j} + v_{i,j}\sum_{k=1}^{M} B_{j,k}^{(1)}T_{i,k}\right)^{n-1},$$

where $[A_1]$, $[A_2]$, $[B_1]$, $[B_2]$, $[C_1]$, $[C_2]$ and $[D_1]$ are the submatrices of Eq. (18) which represent the various differential operators that appear in the DQ approximation. The unknown field variables are the velocities (u, v), vorticity (ω) and temperature (T). The load vectors are the $[f_u]$, $[f_v]$, $[f_\omega]$ and $[f_T]$.

The velocity boundary condition can be computed as

$$\begin{aligned} &u_{1,j} = 0, \quad u_{L,j} = 0, \quad u_{i,1} = 0, \quad u_{i,M} = 1, \\ &v_{1,j} = 0, \quad v_{L,j} = 0, \quad v_{i,1} = 0, \quad v_{i,M} = 0 \\ &\quad \text{for } i = 1, \ldots, L \text{ and } j = 1, \ldots, M. \end{aligned} \tag{19}$$

The vorticity values at boundary wall expressed in terms of velocity gradients by Eq. (11) can also be approximated by the DQ method as follows:

$$\begin{aligned} &\omega_{i,j} - \sum_{k=1}^{L} A_{i,k}^{(1)} v_{k,j} + \sum_{k=1}^{M} B_{j,k}^{(1)} u_{i,k} = 0 \\ &\quad \text{for } i = 1, \ldots, L, \text{ and } j = 1 \text{ or } j = M \\ &\quad \text{for } j = 2, \ldots, M-1, \text{ and } i = 1 \text{ or } i = L. \end{aligned} \tag{20}$$

The Dirichlet temperature boundary conditions at the left and the right walls of the square cavity can be represented as

$$T_{1,j} = 1, \quad T_{L,j} = 0. \tag{21}$$

The adiabatic boundary conditions on the top and bottom sides of 2D natural convection in a cavity can be derived in the DQ form as [11]

$$(B^{(1)}_{1,1}B^{(1)}_{M,M} - B^{(1)}_{M,1}B^{(1)}_{1,M})T_{i,1} - \sum_{k=2}^{M-1}(B^{(1)}_{1,M}B^{(1)}_{M,k} - B^{(1)}_{M,M}B^{(1)}_{1,k})T_{i,k} = 0, \tag{22a}$$

$$(B^{(1)}_{1,M}B^{(1)}_{M,1} - B^{(1)}_{M,M}B^{(1)}_{1,1})T_{i,M} - \sum_{k=2}^{M-1}(B^{(1)}_{M,k}B^{(1)}_{1,1} - B^{(1)}_{1,k}B^{(1)}_{M,1})T_{i,k} = 0$$
$$\text{for } i = 2, \ldots, L-1, \quad j = 1, 2, \ldots, M. \tag{22b}$$

It should be noted that Eqs. (22a), (22b) also involve the implicit scheme for the Neumann boundary conditions. The simultaneous equations resulting from the global matrix system of Eq. (18) are solved using a bi-conjugate iterative equation solver [10]. Since the coefficient values are sparse not only for submatrices but also for the global matrix system as expressed in Eq. (18), only the non-zero entries are stored in a column storage format. The numerical solution procedures used here can be briefly described as follows:

1. Get initial conditions and boundary conditions.
2. Solve the submatrices of Eq. (18).
3. Compute all the non-zero entries in a column storage format in order to solve Eq. (18) efficiently.
4. As far as boundary conditions are concerned, we used the velocity boundary condition of Eq. (19), the vorticity definition of Eq. (20) and temperature boundary conditions of Eqs. (21), (22) to satisfy the system of Eq. (18).
5. Eq. (18) is advanced in time to solve the unknown velocity, vorticity and temperature.
6. Check for the convergence of the velocity, vorticity and temperature components in the present study. We used the velocity, vorticity and temperature components at the previous time step as the initial guess for the next iteration. The computations are carried out until steady state conditions are reached. The convergence criteria used in the time loop to achieve steady state conditions are

$$|(u^{n+1} - u^n)/u^n| \leqslant 10^{-6}, \quad |(v^{n+1} - v^n)/v^n| \leqslant 10^{-6}, \quad |(\omega^{n+1} - \omega^n)/\omega^n| \leqslant 10^{-6},$$
$$|(T^{n+1} - T^n)/T^n| \leqslant 10^{-6}. \tag{23}$$

For the DQ method, the mesh point distribution in the two spatial coordinates is expressed as [11]

$$x_i = \frac{\cos[\pi/(2L)] - \cos[(2i-1)\pi/(2L)]}{\cos[\pi/(2L)] - \cos[(2L-1)\pi/(2L)]}L_x, \quad i = 1, 2, \ldots, L$$
$$y_j = \frac{\cos[\pi/(2M)] - \cos[(2j-1)\pi/(2M)]}{\cos[\pi/(2M)] - \cos[(2M-1)\pi/(2M)]}L_y, \quad j = 1, 2, \ldots, M \tag{24}$$

where L, M are the numbers of grid points in the x, y directions, respectively. L_x is the length in the x direction, and L_y is the width in the y direction, respectively.

5. Results and discussion

A numerical model was developed to validate the accuracy for the solutions of 2D natural convection in a cavity as shown in Fig. 1. The no-slip boundary conditions of the velocities at boundary walls are assumed. Temperature equal to 1 and 0 are assumed at the left and the right walls, respectively. Adiabatic conditions are assumed on the top and bottom sides of the cavity. The aspect ratios of height and length is defined as H/L, and H/L varying from 1 to 3 was undertaken in the present work. In order to establish benchmark solution, the obtained numerical results are compared

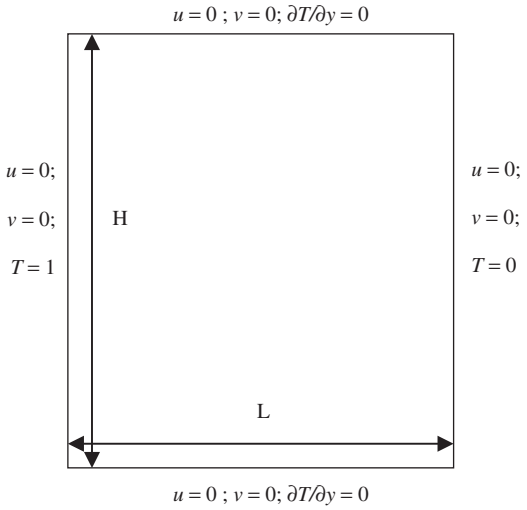

Fig. 1. Layout of the problem.

Table 1
Grid-independence study results of natural convection in a square cavity for $Ra = 10^3$ and 10^4

Ra	10^3				10^4			
Method	DQ	DQ	DQ	Bench. [16]	DQ	DQ	DQ	Bench. [16]
Mesh size	21 × 21	25 × 25	31 × 31	81 × 81	21 × 21	25 × 25	31 × 31	81 × 81
Nu_{avg}	1.118	1.118	1.118	1.118	2.244	2.244	2.244	2.243
Error (%)	0	0	0		0.045	0.045	0.045	

with the results due to Vahl Davis [15] who used a grid size of 81 × 81 in a square cavity. The significant parameter for natural convection is to compute the Nusselt number as follows:

1. The Nusselt number on the vertical boundary at $x = 0$, evaluated as

$$Nu_0 = \int_0^H \frac{\partial T}{\partial x}\,\mathrm{d}y.$$

2. The average Nusselt number throughout the cavity, evaluated as

$$Nu_{\mathrm{avg}} = \frac{1}{(H/L)} \int_0^L Nu_0\,\mathrm{d}x.$$

5.1. Grid-independence study

For the case of a natural convection in a square cavity, the average Nusselt number throughout the cavity is considered as important parameters for comparison purposes. Tables 1 and 2 depict the comparisons of the above parameters obtained in the present work for $10^3 \leqslant Ra \leqslant 10^6$ with the benchmark solution obtained using streamfunction–vorticity formulation in [15]. The present study produces almost the same results as obtained in [15]. However, it can be observed that the present scheme used three grid sizes to produce the same results compared to the benchmark solution. From the results obtained, one can observe the computational grid was refined successively from 21×21 to 25×25 and 31×31, in which very accurate results are obtained in all the three grids system. Thereby, the present coupled numerical algorithm

Table 2
Grid-independence study results of natural convection in a square cavity for $Ra = 10^5$ and 10^6

Ra	10^5				10^6			
Method	DQ	DQ	DQ	Bench. [16]	DQ	DQ	DQ	Bench. [16]
Mesh size	21×21	25×25	31×31	81×81	21×21	25×25	31×31	81×81
Nu_{avg}	4.520	4.521	4.521	4.519	8.820	8.823	8.823	8.8
Error (%)	0.022	0.044	0.044		0.227	0.261	0.261	

Table 3
Comparison of CPU time (s) for different Rayleigh number

	Mesh size	Δt	CPU time (s)
$Ra = 10^3$	21×21	0.01	45
	25×25	0.01	122
	31×31	0.01	601
$Ra = 10^4$	21×21	0.005	120
	25×25	0.005	372
	31×31	0.005	1201
$Ra = 10^5$	21×21	0.0002	451
	25×25	0.0002	1251
	31×31	0.0002	3202
$Ra = 10^6$	21×21	0.00002	1531
	25×25	0.00002	4252
	31×31	0.00002	12052

based on the velocity–vorticity form of the Navier–Stokes equations and the DQ method computes the average Nusselt number throughout the cavity consistently with grid refinement.

5.2. Results on flow and hydrothermal characteristics

As far as the CPU time for different Rayleigh number is concerned, Table 3 summarizes the total CPU time of different Rayleigh number for three grids system. From the above computed tabulation, the CPU time increases as Rayleigh number increased. Also, the computation of CPU time is increasing from the different numbers of grid nodes 21^2–25^2 and 31^2. In Table 4, we present comparisons of an excellent agreement with the results obtained in [15] for $Ra = 10^3$, 10^4, 10^5, and 10^6. For the case of higher Rayleigh number equal to 10^7, the evaluations of the maximum Nusselt number and minimum Nusselt number as well as average Nusselt number are presented in Table 4, respectively. The obtained results indicate that present work is capable of handling high Rayleigh number without difficulties. The present coupled numerical scheme is further demonstrated by plotting the velocity, temperature, vorticity and streamline contours as shown in Fig. 2 by using a grid of 31×31 points for $Ra = 10^3$, 10^4, 10^5, 10^6 and 10^7, respectively.

After successfully validating the present algorithm for natural convection in a square cavity, we further analyze the different H/L aspect ratios of 2 and 3. For the case of the different ratios in a cavity, Ismail and Scalon [8] developed a finite element method for numerical solutions of free convection in a cavity with side walls maintained at constant but different temperatures over a wide range of Rayleigh number ($10^3 \leqslant Ra \leqslant 10^6$) and different L/H aspect ratios. Table 5 displays the comparison of the Nusselt number predicated in a cavity for various H/L aspect ratios. The increase in the values of average Nusselt number with increase in Rayleigh number has been accurately solved as expected trend. From the tabulated results it can be noted that the present model obtained the benchmark solution with a coarser grid for all five values of Rayleigh number and different H/L aspect ratios varying from 1 to 3. Additionally, the distributions of velocity, temperature and vorticity fields are plotted in Figs. 3–5 for $Ra = 10^5$, 10^6 and 10^7 in the case of $H/L = 2/1$, respectively.

Table 4
Numerical results of natural convection in a square cavity for different average Nusselt number

	$Nu_{\max}$	$Nu_{\min}$	Nu_{avg}
$Ra = 10^3$			
Bench. [16]	1.505	0.692	1.118
(Position)	($y = 0.092$)	($y = 1$)	
Present (DQ)	1.506	0.691	1.118
Error	0.066%	0.145%	0%
(Position)	($y = 0.103$)	($y = 1$)	
$Ra = 10^4$			
Bench. [16]	3.528	0.586	2.243
(Position)	($y = 0.143$)	$y = 1$	
Present (DQ)	3.531	0.585	2.244
Error	0.085%	0.171%	0.045%
(Position)	($y = 0.146$)	$y = 1$	
$Ra = 10^5$			
Bench. [16]	7.717	0.729	4.519
(Position)	($y = 0.081$)	($y = 1$)	
Present (DQ)	7.708	0.728	4.521
Error	0.117%	0.137%	0.044%
(Position)	($y = 0.095$)	($y = 1$)	
$Ra = 10^6$			
Bench. [16]	17.925	0.989	8.8
(Position)	($y = 0.0378$)	($y = 1$)	
Present (DQ)	17.524	0.982	8.823
Error	2.237%	0.708%	0.261%
(Position)	($y = 0.043$)	($y = 1$)	
$Ra = 10^7$			
Present (DQ)	39.287	1.250	16.641
(Position)	($y = 0.024$)	($y = 1$)	

Further, when $H/L = 3/1$ for the distributions of velocity vector, temperature and vorticity fields are shown in Figs. 6–8 , respectively. As the Rayleigh number increases, one can observe the rapid changes occurring in the velocity vectors indicating an increase of the convection participation in the heat transfer process for all the cases. The increase of vorticity values near the isothermal walls indicate that a near-stagnant interior core occurs along with the distinct boundary layers near the end walls with increase in the values of the Rayleigh number. As the gap height increases, it means that the aspect ratios H/L increase, for all the cases of high Rayleigh number the heat transfer by conduction is reduced while the natural convection effect starts to get stronger. As the convection spreads to the entire cavity, we observe the formation of circulating cells adjacent to the corners of the cavity. The increase in the fluid convection process with increase in Rayleigh number results in the thinning of the boundary layers as observed in above figures. In the present formulation, the vortex which was originally in circular pattern for $Ra = 10^3$ now changes its shape to elliptical forms with increase in the value of the Rayleigh number. From the results obtained, we can note the onset of vortex domination throughout the entire cavity, thus affecting the flow field. The above figures also indicate the increase in the value of the constant vorticity lines is observed as the value of the Rayleigh number increases.

In Fig. 9 , we exhibit comparisons of the variations of y–u and x–v velocity profile plots for $10^3 \leqslant Ra \leqslant 10^7$ and H/L aspect ratios varying from 1 to 3, respectively. Since all no-slip velocity boundary conditions are enforced at boundary walls for the natural convection problem, a symmetric velocity distribution is expected in the above figure. For the cases of the $Ra = 10^3$ at different aspect ratios varying from 1 to 3, there is not enough convective motion of the fluid within the cavity due to the viscous force domination, which is delineated by a line which is almost vertical. As the Rayleigh number increases, the buoyancy force increases giving rise to an effective fluid convection, which will lead to a circulatory gyre pattern. The circulatory gyre pattern is indicated by the positive and negative u-velocity values along the symmetric vertical plane as observed in the above figure. The velocity value reaches its maximum for $Ra = 10^7$

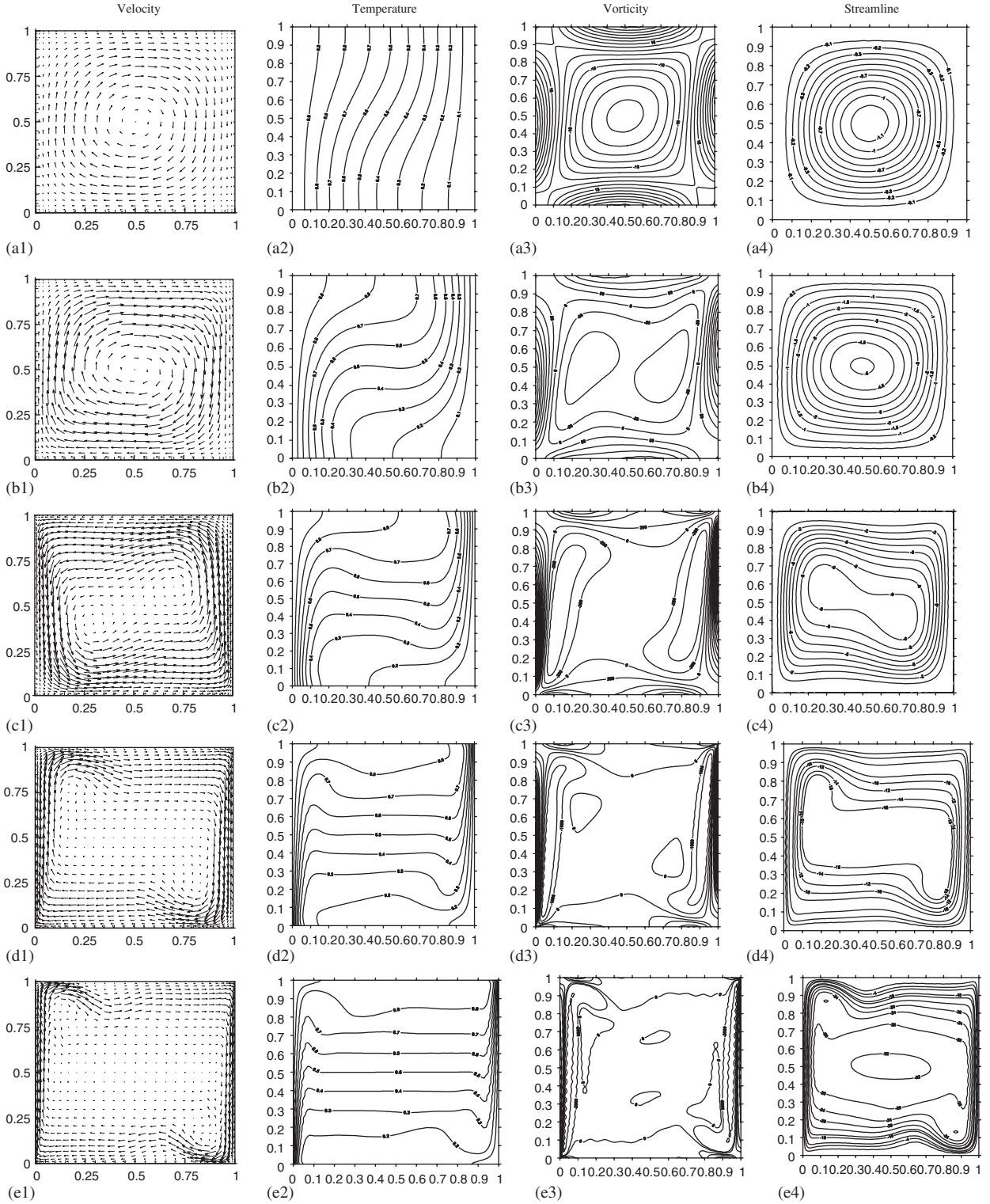

Fig. 2. Distributions of velocity, temperature, vorticity and streamline for a 2D square cavity at different Ra number for $Ra = 10^3$ (a1–a4), $Ra = 10^4$ (b1–b4), $Ra = 10^5$ (c1–c4), $Ra = 10^6$ (d1–d4), $Ra = 10^7$ (e1–e4), $H/L = 1/1$.

Table 5
Nusselt number predicated in a cavity for various H/L aspect ratios

	Mesh size	Nu_{max}	Nu_{min}	Nu_{avg}
$Ra = 10^3$	31×31			
DQ ($H/L = 1/1$)		1.506	0.691	1.118
(Position)		($y = 0.103$)	$y = 1$	
DQ ($H/L = 2/1$)	31×61	1.897	0.487	1.191
(Position)		($y = 0.191$)	($y = 2$)	
DQ ($H/L = 3/1$)	31×91	1.940	0.459	1.146
(Position)		($y = 0.201$)	($y = 3$)	
$Ra = 10^4$	31×31			
DQ ($H/L = 1/1$)		3.531	0.585	2.244
(Position)		($y = 0.146$)	($y = 1$)	
DQ ($H/L = 2/1$)	31×61	4.272	0.340	2.354
(Position)		($y = 0.191$)	($y = 2$)	
DQ ($H/L = 3/1$)	31×91	4.523	0.234	2.232
(Position)		($y = 0.201$)	($y = 3$)	
$Ra = 10^5$	31×31			
DQ ($H/L = 1/1$)		7.708	0.728	4.521
(Position)		($y = 0.095$)	($y = 1$)	
DQ ($H/L = 2/1$)	31×61	8.471	0.473	4.301
(Position)		($y = 0.086$)	($y = 2$)	
DQ ($H/L = 3/1$)	31×91	8.644	0.382	4.059
(Position)		($y = 0.090$)	($y = 3$)	
$Ra = 10^6$	31×31			
DQ ($H/L = 1/1$)		17.524	0.982	8.823
(Position)		($y = 0.043$)	($y = 1$)	
DQ ($H/L = 2/1$)	31×61	19.168	0.643	7.904
(Position)		($y = 0.034$)	($y = 2$)	
DQ ($H/L = 3/1$)	31×91	19.324	0.521	7.269
(Position)		($y = 0.033$)	($y = 3$)	
$Ra = 10^7$	31×31			
DQ ($H/L = 1/1$)		39.287	1.250	16.641
(Position)		($y = 0.024$)	($y = 1$)	
DQ ($H/L = 2/1$)	31×61	40.898	0.803	14.519
(Position)		(0.022)	($y = 2$)	
DQ ($H/L = 3/1$)	31×91	40.840	0.593	13.292
(Position)		($y = 0.033$)	($y = 3$)	

with steep velocity gradients at the middle of the vertical central plane. This is because at higher values of the Rayleigh number the non-linear characteristic of fluid convection becomes more dominant in the flow field. A similar trend is observed with the v-velocity variation seen from Fig. 9.

The Nusselt number is an important non-dimensional parameter in convective heat transfer. Thus, the Nusselt number for several H/L aspect ratios at different Rayleigh number is briefly sketched in Fig. 10, respectively. It is interesting to indicate that the maximum values of the Nusselt number along the y direction is not at bottom wall, but close to the bottom wall. An initial look at the range of the Nusselt number values shown in these figures clearly indicates that the Nusselt number increases with increase in the value of the Rayleigh number as expected. When convective heat transport reaches minimum at lower value of Rayleigh number up to 10^4, the value of the Nusselt number is smaller compared to higher Rayleigh number. The pronounced convective heat transfer due to the increase in value of the Rayleigh number to 10^7 is vividly indicated in Fig. 10. The present coupled numerical algorithm has accurately predicted the convective heat transport process inside the cavity. Thus, it is convinced that the present scheme is an effective and robust method for predicating the heat transfer problems when the governing equations in velocity–vorticity form are used as a fully coupled system of equations.

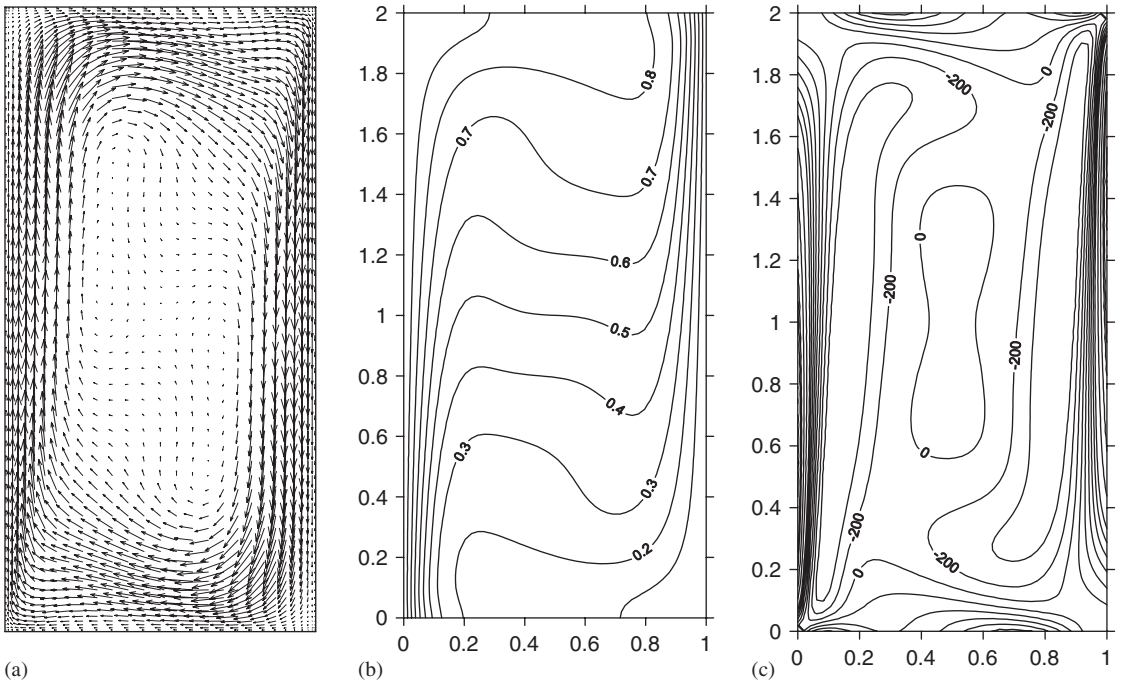

Fig. 3. Distributions of (a) velocity, (b) temperature and (c) vorticity for $Ra = 10^5$, $H/L = 2/1$.

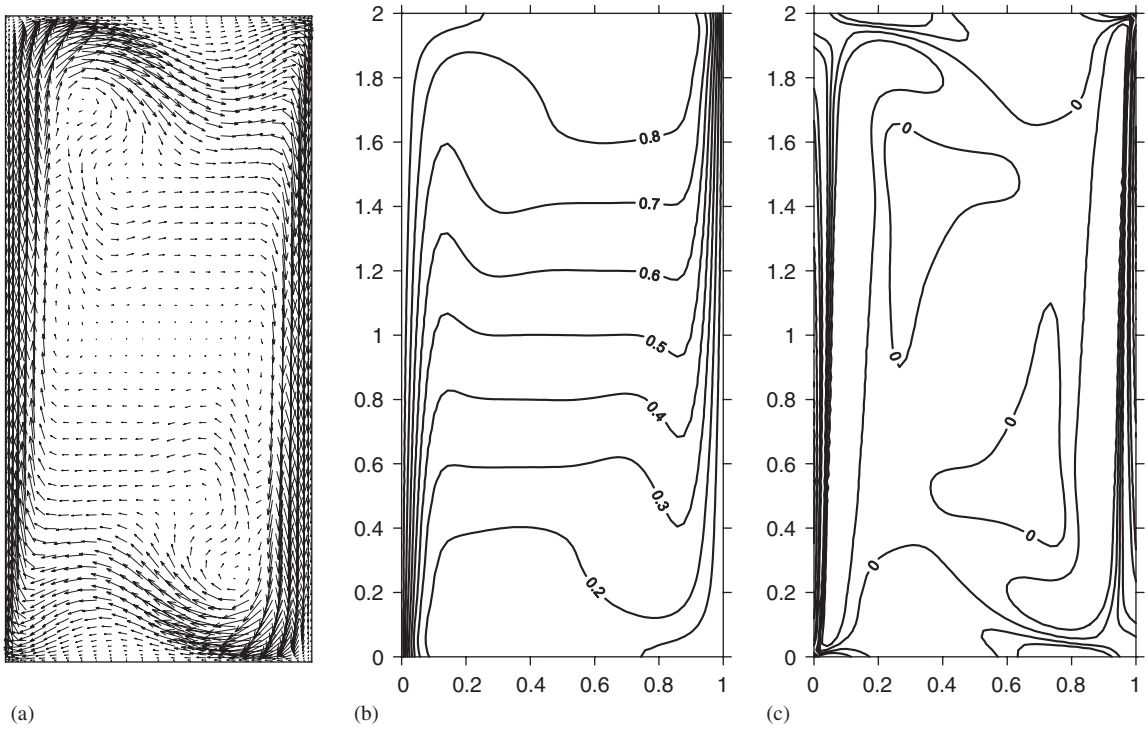

Fig. 4. Distributions of (a) velocity, (b) temperature and (c) vorticity for $Ra = 10^6$, $H/L = 2/1$.

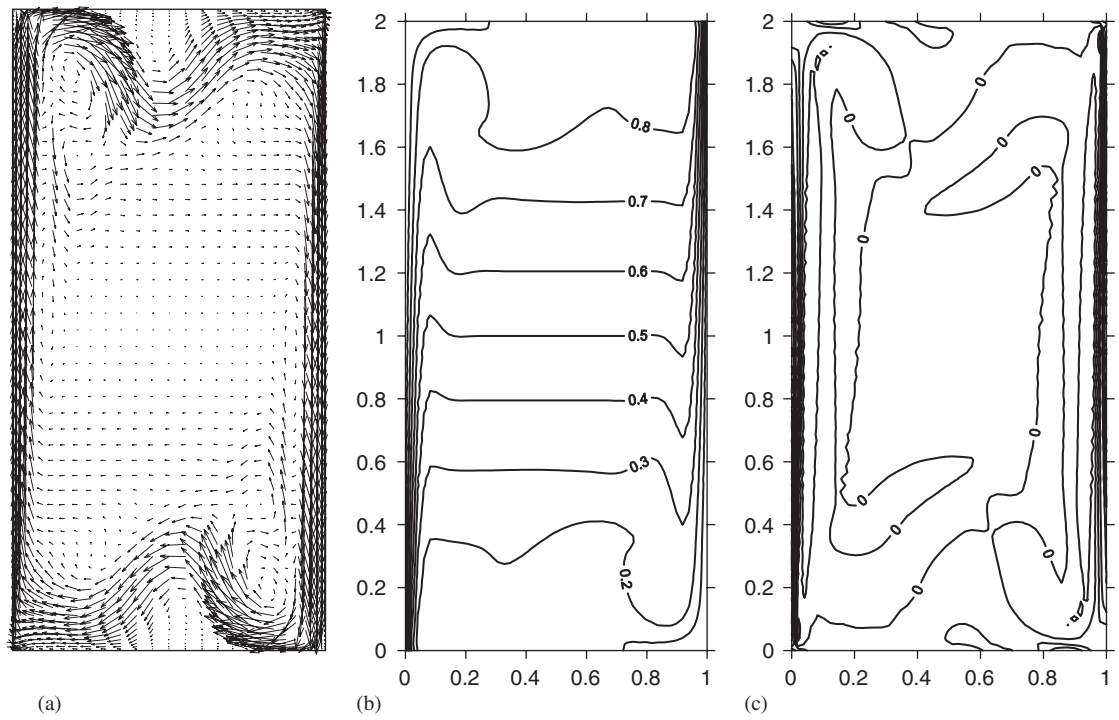

Fig. 5. Distribution of (a) velocity, (b) temperature and (c) vorticity for $Ra = 10^7$, $H/L = 2/1$.

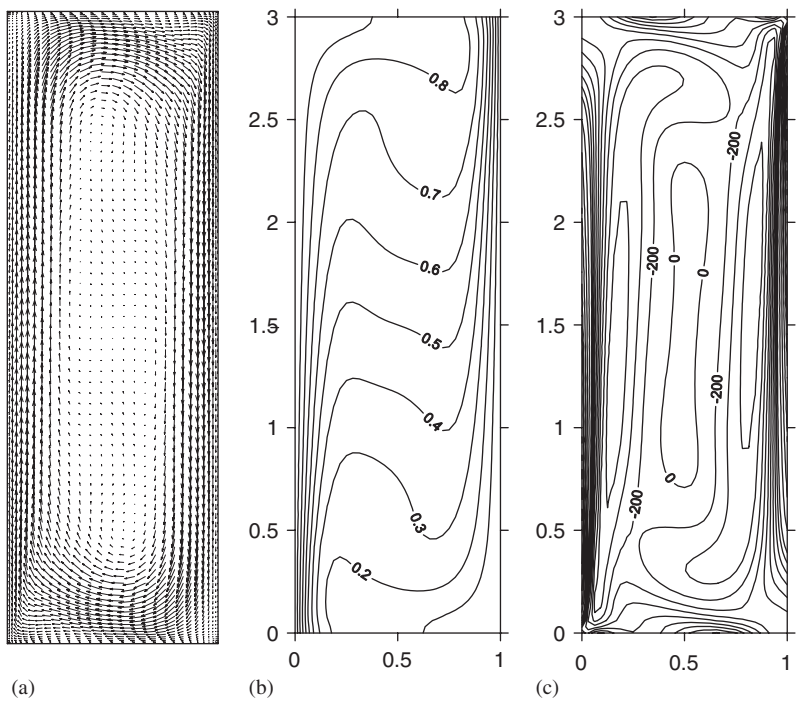

Fig. 6. Distributions of (a) velocity, (b) temperature and (c) vorticity for $Ra = 10^5$, $H/L = 3/1$.

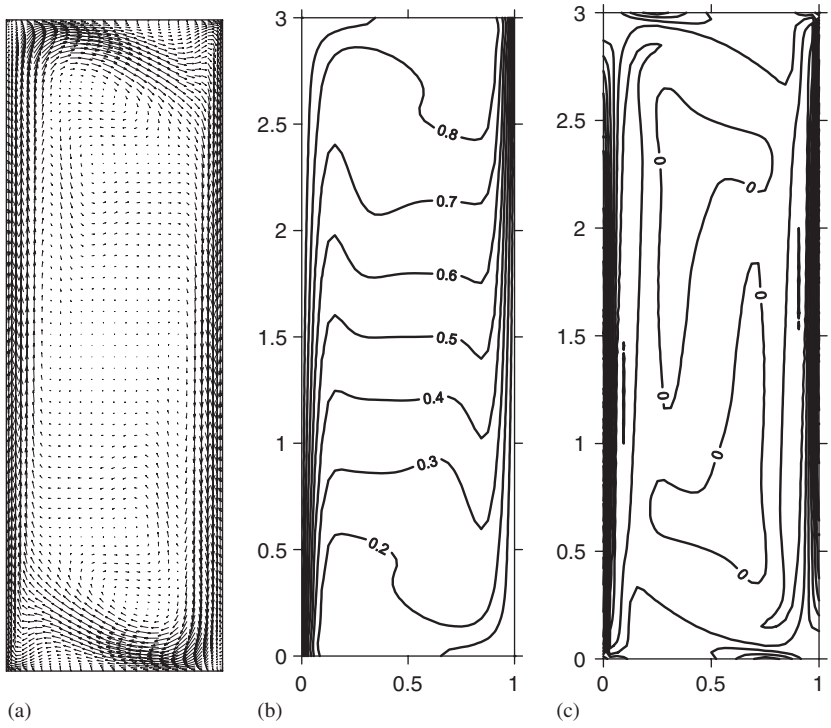

Fig. 7. Distributions of (a) velocity, (b) temperature and (c) vorticity for $Ra = 10^6$, $H/L = 3/1$.

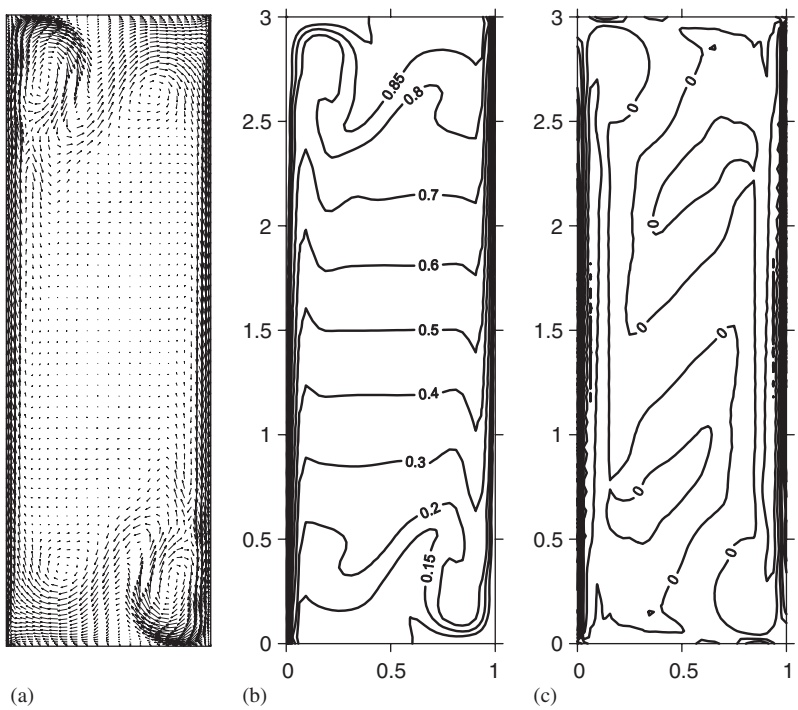

Fig. 8. Distributions of (a) velocity, (b) temperature and (c) vorticity for $Ra = 10^7$, $H/L = 3/1$.

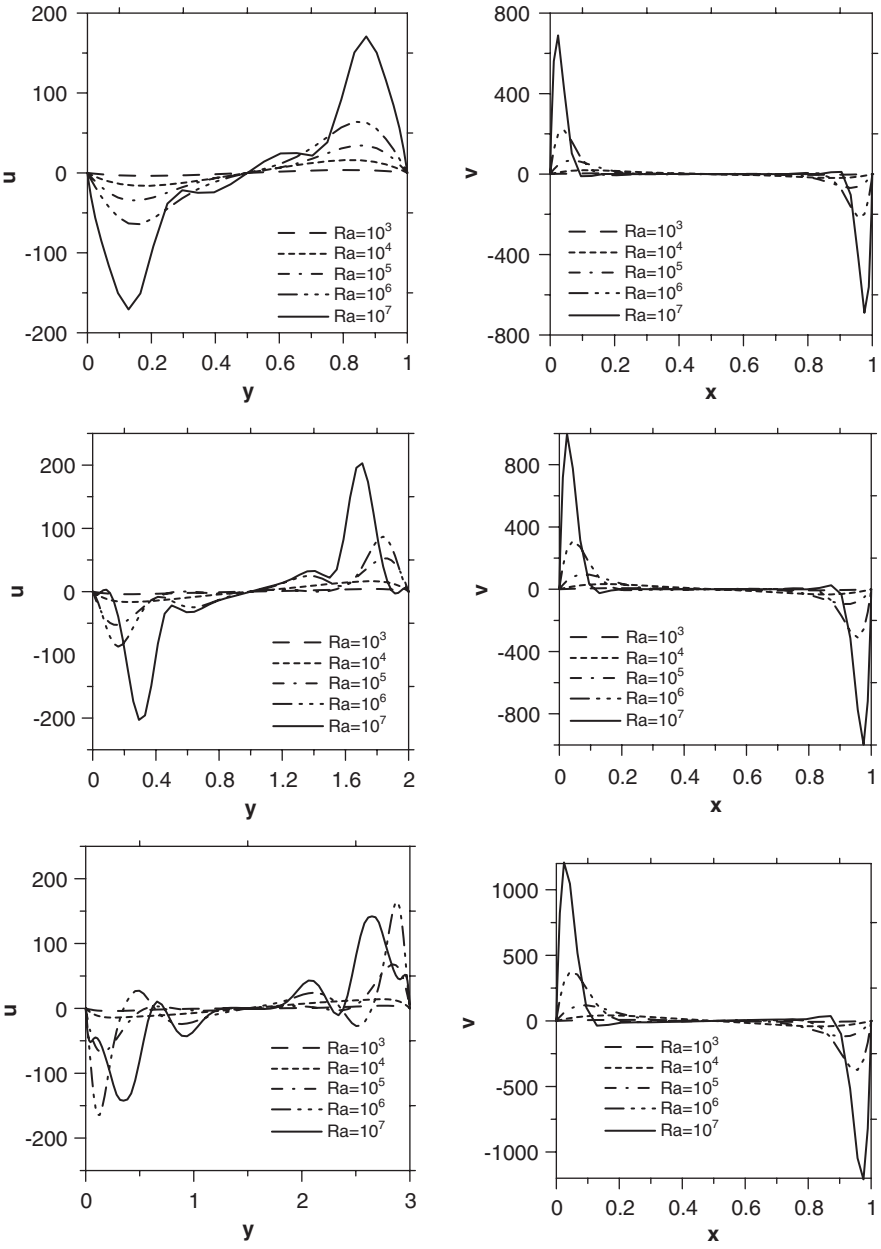

Fig. 9. Centerline velocity profiles of the symmetry for $10^3 \leqslant Ra \leqslant 10^7$.

6. Conclusions

The 2D Navier–Stokes equations in velocity–vorticity form are numerically solved using the DQ method and the numerical algorithm developed has been successfully implemented to study natural convection in a differentially heated cavity. Higher-order polynomial approximation used for discretizing the partial differential derivatives in the DQ method has been effectively used to obtain accurate numerical results while solving the velocity–vorticity form of the Navier–Stokes equations. More importantly the higher-order polynomial approximation used in the DQ method enabled the computation of the vorticity values at boundary more accurately. The coupled solution procedure followed in the present scheme completely eliminated the explicit specification of the vorticity boundary values without involving

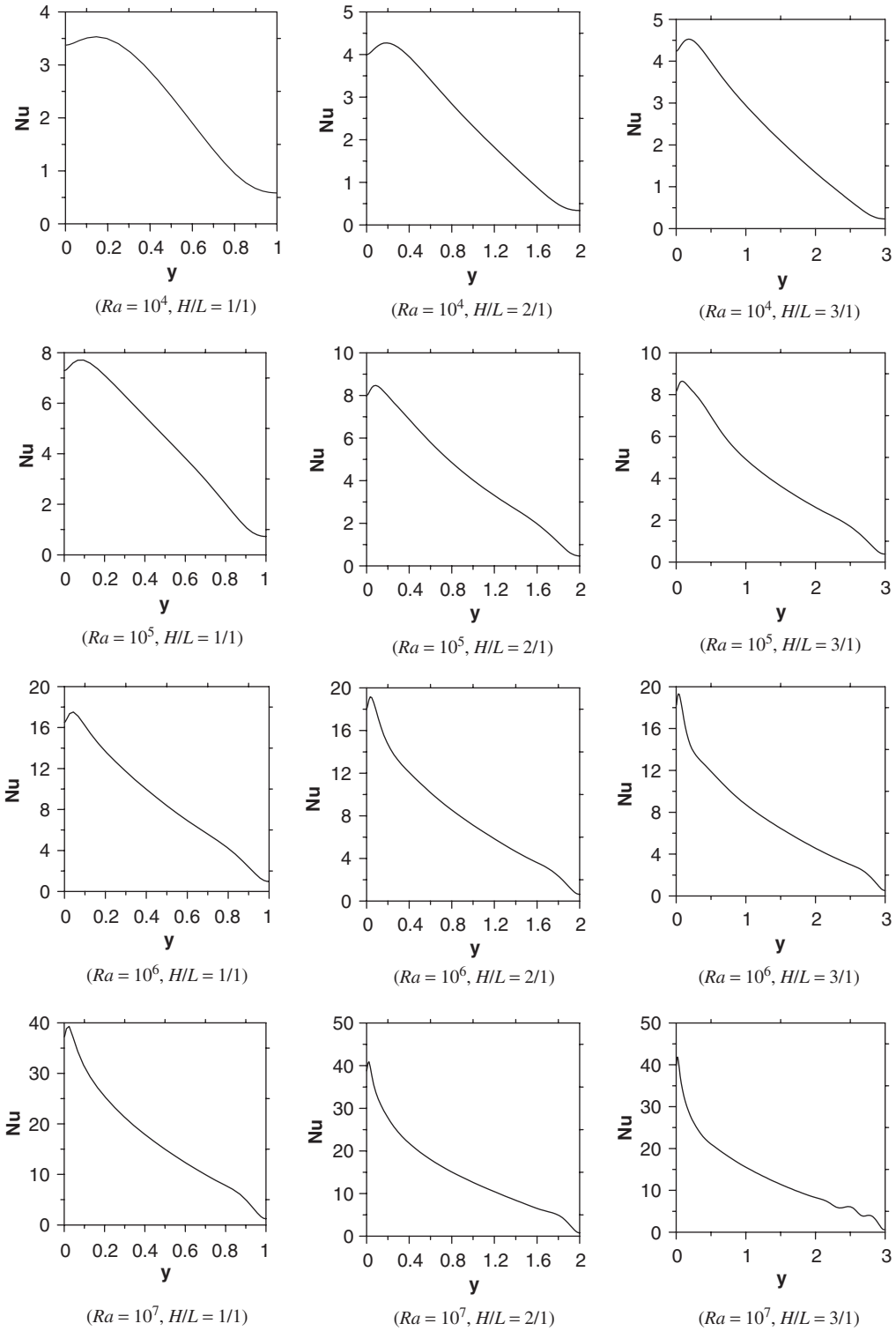

Fig. 10. Nusselt number for several H/L aspect ratios at different Ra numbers.

any iterative procedure. Test results for natural convection in a differentially heated cavity indicates that:

- Velocity vector contours and temperature contours plotted and the Nusselt number variations for $10^3 \leqslant Ra \leqslant 10^7$ in a square cavity are in quantitative agreement with the results available in the literature.
- Vorticity contours plotted show the increase in vorticity values with increase in the Rayleigh number in terms of the variation of the aspect ratios H/L of the cavity.
- Since the computer memory and computational effort are directly proportional to the number of grid points used, the present numerical scheme indicates that a significant saving in computational time can be achieved.
- The present study proposed a new numerical scheme to solve two-dimensional Navier–Stokes equations by efficiently exploiting the advantages of both the velocity–vorticity form of the Navier–Stokes equations and the DQ method.

Acknowledgments

The support under Grants NSC 94-2218-E-464-001, 93-2611-E-002-017 and 94-2211-E-464-003 by the National Science Council of Taiwan are gratefully acknowledged.

References

[1] G.K. Batchelor, An Introduction to Fluid Mechanics, Cambridge University Press, Cambridge, UK, 1967.
[2] R.E. Bellman, B.G. Kashef, J. Casti, Differential quadrature: a technique for the rapid solution of nonlinear partial differential equations, J. Comput. Phys. 10 (1972) 40–52.
[3] O. Daube, Resolution of the 2D Navier–Stokes equations in velocity–vorticity form by means of an influence matrix technique, J. Comput. Phys. 103 (1992) 402–414.
[4] H. Ding, C. Shu, K.S. Yeo, D. Xu, Development of least-square-based two-dimensional finite-difference schemes and their application to simulate natural convection in a cavity, Comput. & Fluids 33 (2004) 137–154.
[5] H. Fasel, Investigation of the stability of boundary layers by a finite-difference model of the Navier–Stokes equations, J. Fluid Mech. 78 (1976) 355–383.
[6] P.M. Gresho, R.L. Sani, Advection–diffusion and isothermal laminar flow, Incompressible Flow and the Finite Element Method, vol. 1. Wiley, New York, 2002.
[7] G. Guj, F. Stella, A vorticity–velocity method for the numerical solution of 3D incompressible flows, J. Comput. Phys. 106 (1993) 286–298.
[8] K.A.R. Ismail, V.L. Scalon, A finite element free convection model for the side wall heated cavity, Internat. J. Heat Mass Transfer 43 (2000) 1373–1389.
[9] D.C. Lo, K. Murugesan, D.L. Young, Numerical solution of three-dimensional velocity–vorticity Navier–Stokes equations by finite difference method, Internat. J. Numer. Methods Fluids 47 (2005) 1469–1487.
[10] W.H. Press, S.A. Teukolsky, W.T. Vetterling, B.P. Flannery, Numerical Recipes in Fortran 90, second ed., Cambridge University Press, New York, 1996.
[11] C. Shu, Differential Quadrature and Its Application in Engineering, Springer, London, 2000.
[12] C. Shu, H. Ding, K.S. Yeo, Local radial basis function-based differential quadrature method and its application to solve two-dimensional incompressible Navier–Stokes equations, Comput. Methods Appl. Mech. Eng. 192 (2003) 941–954.
[13] C. Shu, B.E. Richards, Application of generalized differential quadrature to solve 2-dimensional incompressible Navier–Stokes equations, Internat. J. Numer. Methods Fluids 15 (1992) 791–798.
[14] C. Shu, H. Xue, Comparison of two approaches for implementing stream function boundary conditions in DQ simulation of natural convection in a square cavity, Internat. J. Heat Fluid Flow 19 (1998) 59–68.
[15] G. de Vahl Davis, Natural convection of air in a square cavity, a bench mark numerical solution, Internat. J. Numer. Methods Fluids 3 (1983) 249–264.
[16] J.M. Vanel, R. Peyret, P. Bontoux P, in: K.W. Morton, M.J. Baines (Eds.), Numerical Methods for Fluid Dynamics, vol. II, Clarendon Press, Oxford, 1986, pp. 463–475.
[17] K.L. Wong, A.J. Baker, A 3D incompressible Navier–Stokes velocity–vorticity weak form finite element algorithm, Internat. J. Numer. Methods Fluids 38 (2002) 99–123.
[18] X.H. Wu, J.Z. Wu, J.M. Wu, Effective vorticity–velocity formulations for three-dimensional incompressible viscous flows, J. Comput. Phys. 122 (1995) 68–82.
[19] Y.L. Wu, G.R. Liu, A meshfree formulation of local radial point interpolation method (LRPIM) for incompressible flow simulation, Comput. Mech. 30 (2003) 355–365.